Journal of Geophysical Research - Solid Earth

Supporting Information for

Stacked magma lenses beneath mid-ocean ridges: insights from new seismic observations and synthesis with prior geophysical and geologic findings

Suzanne M. Carbotte[1], Milena Marjanović[2], Adrien Arnulf[3], Mladen R. Nedimović[4], Juan Pablo Canales[5], Gillean M Arnoux[6]

[1] Department of Marine Geology and Geophysics, Lamont-Doherty Earth Observatory, Columbia University, Palisades, NY, USA

[2]Université de Paris, Institut de Physique du Globe de Paris, CNRS, Paris, France

[3]Jackson School, Institute for Geophysics, University of Texas at Austin, TX, USA

[4]Department of Earth and Environmental Sciences, Dalhousie University, Halifax, Nova Scotia B3H 4R2, Canada

[5]Department of Geology and Geophysics, Woods Hole Oceanographic Institution, Woods Hole, MA, USA

[6]Department of Earth Sciences, University of Oregon, Eugene, OR USA

Contents of this file

Figures S1 to S6

Introduction

Supporting information includes a location map and images of all multi-channel seismic sections used in this study of the Juan de Fuca Ridge. Details on seismic acquisition and

data processing are included in the main text. Interpreted horizons as shown in Figure 4 are included as transparent overlays on the seismic images.

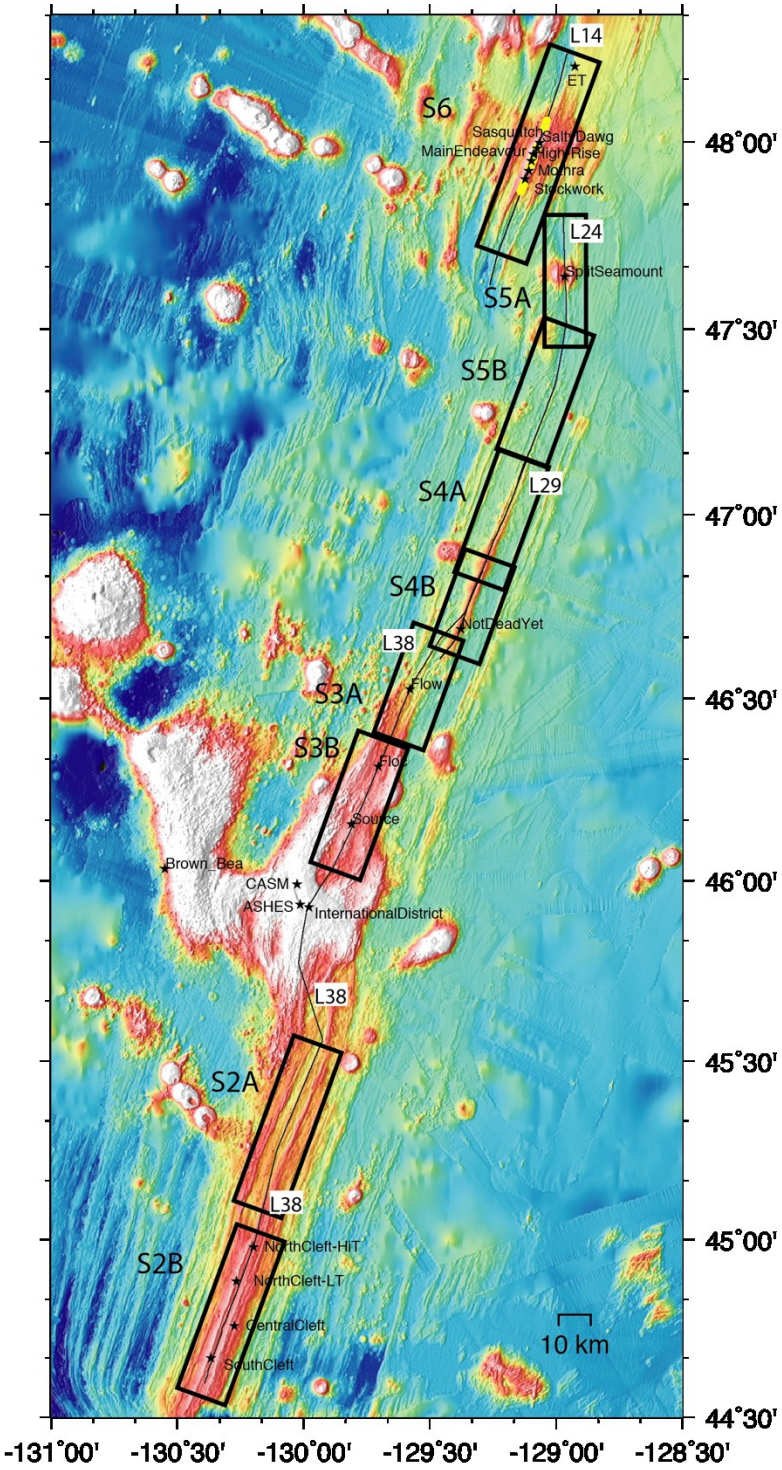

Figure S1. Bathymetric map of the study region showing locations of seismic sections included in supplement. Seismic trackline locations (black line) and numbers (L14, L24, L29 and L38) and hydrothermal vent locations (black stars) and names are indicated (as in Fig. 1). Rectangles show locations of seismic sections in Figures S2-6. The portion of Line 38 crossing Axial Seamount is recently published in Carbotte et al (2020) and is not reproduced here.

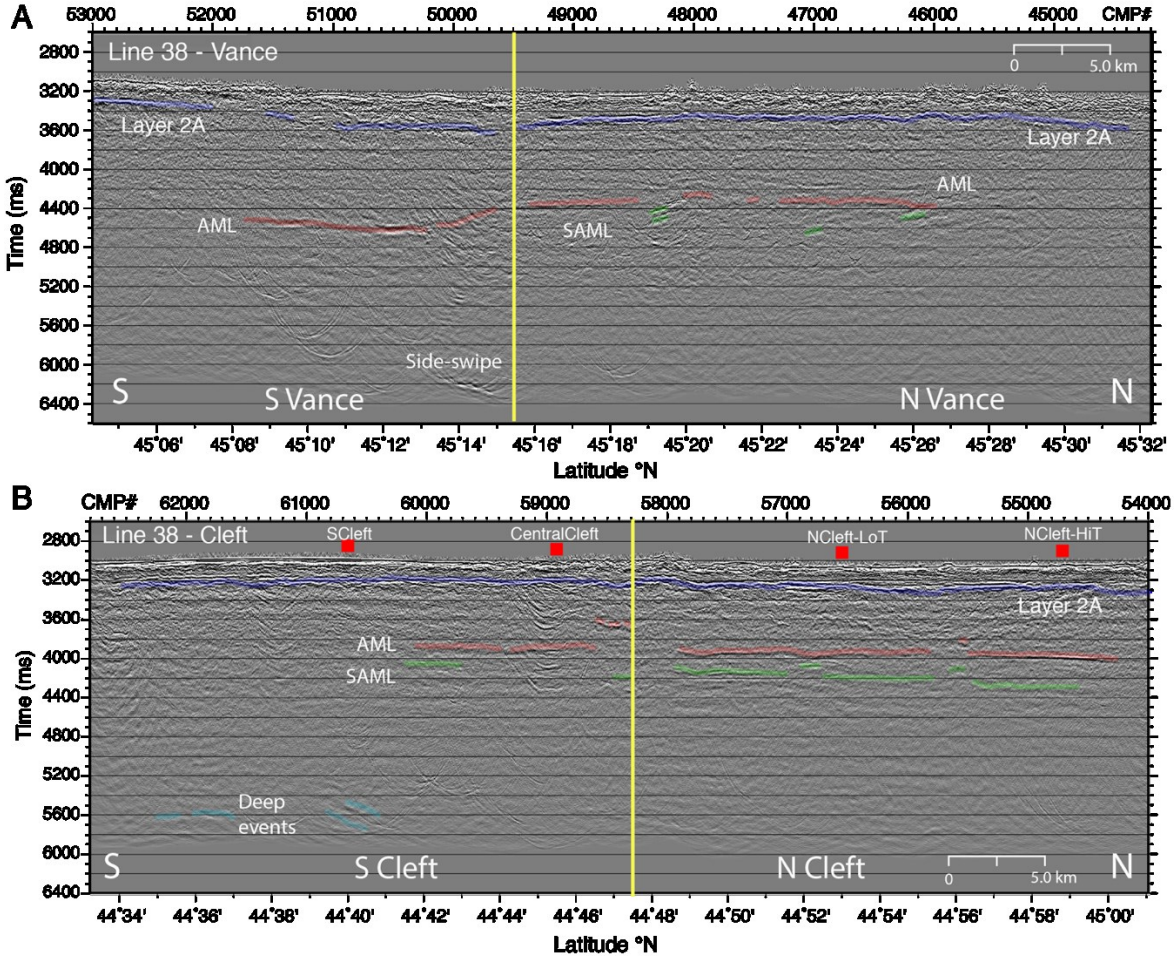

Figure S2. Processed migrated section for line 38 along axis of Vance (top) and Cleft (bottom) segments. Yellow vertical lines indicate boundaries between the two smaller (third-order) spreading segments identified along these two segments. Locations of hydrothermal vents shown with red squares at top of section. Interpreted horizons are superimposed in semi-transparent line with colors as in Figure 4. Note that for south Vance and south Cleft, the along-axis composite in Figure 4 shows the previously published AML interpretation (in purple line) from Canales et al. (2006) which were derived from the more-axially centered seismic lines 42 and 80 acquired within these regions.

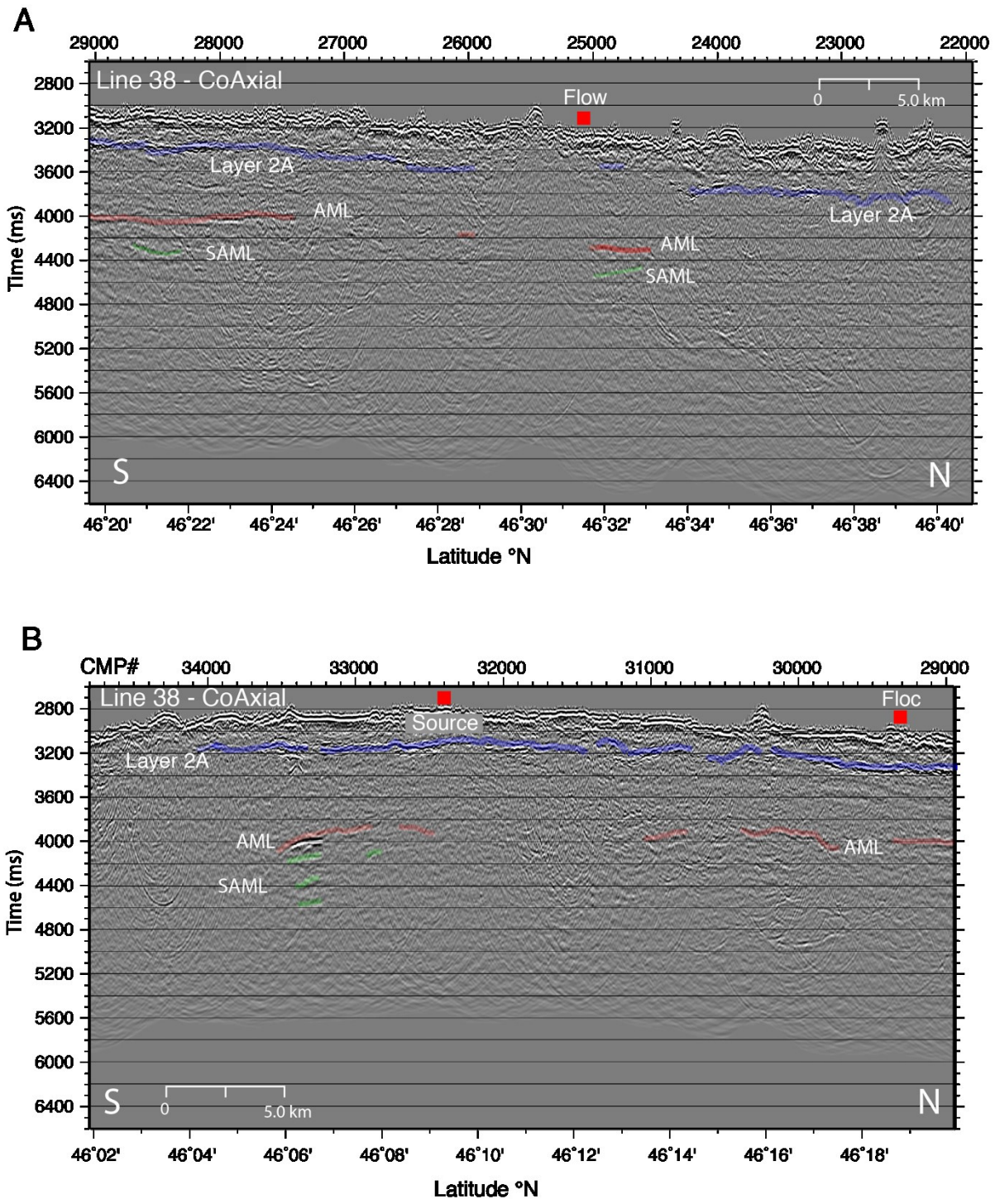

Figure S3. Processed migrated section for line 38 along axis of Co-Axial segment. Locations of hydrothermal vents shown with red squares at top of section. Interpreted horizons are superimposed in semi-transparent line with colors as in Figure 4. A. Part 1 of section from CDP# 21950-29050. B. Part 2 of section from CDP# 28950-34800.

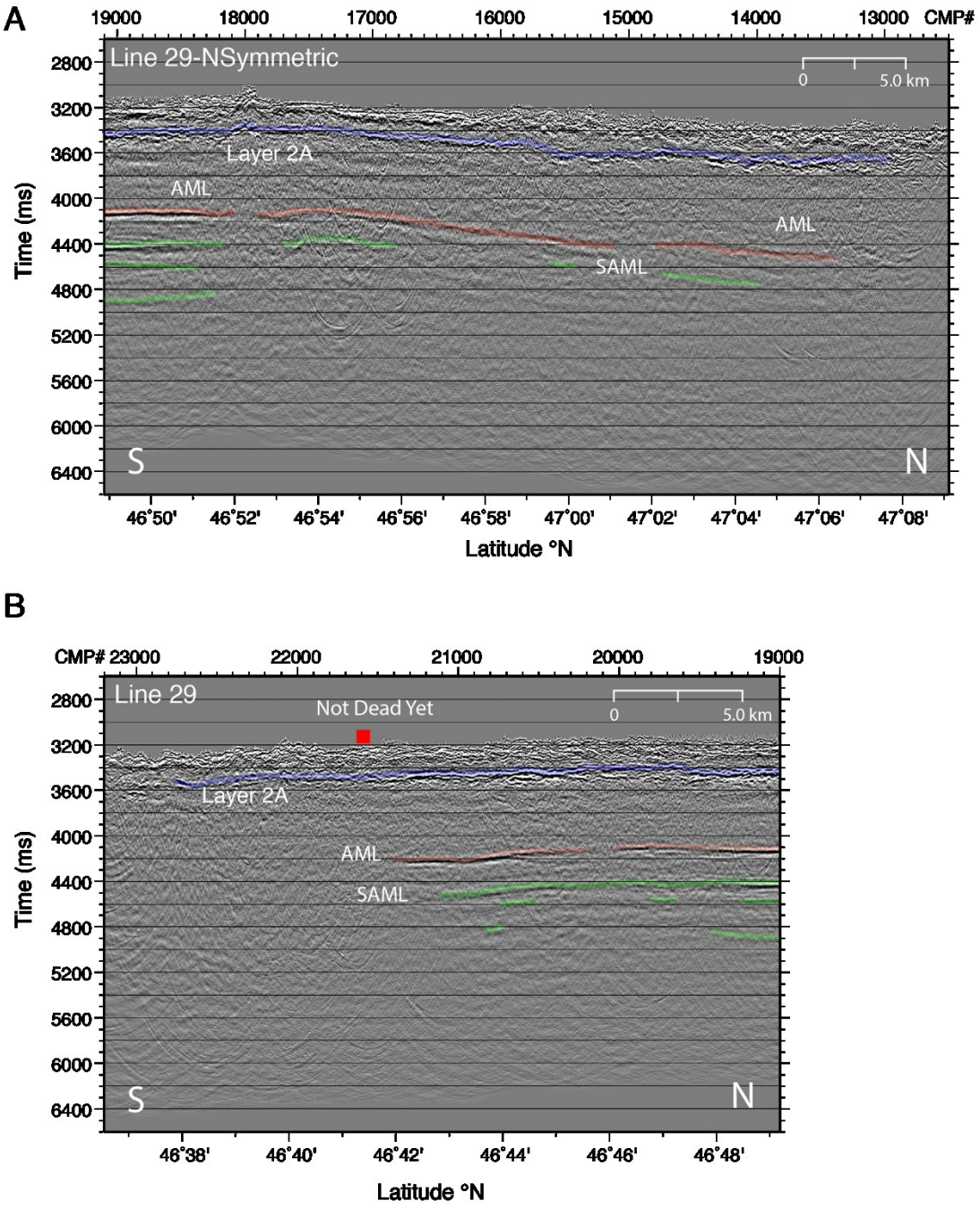

Figure S4. Processed migrated section for line 29 along axis of southern-central Northern Symmetric segment. Locations of hydrothermal vents shown with red squares at top of section. Interpreted horizons are superimposed in semi-transparent line with colors as in Figure 4. A. Part 1 of section from CDP 12500-18900. B. Part 2 of section from CDP 19000-23200.

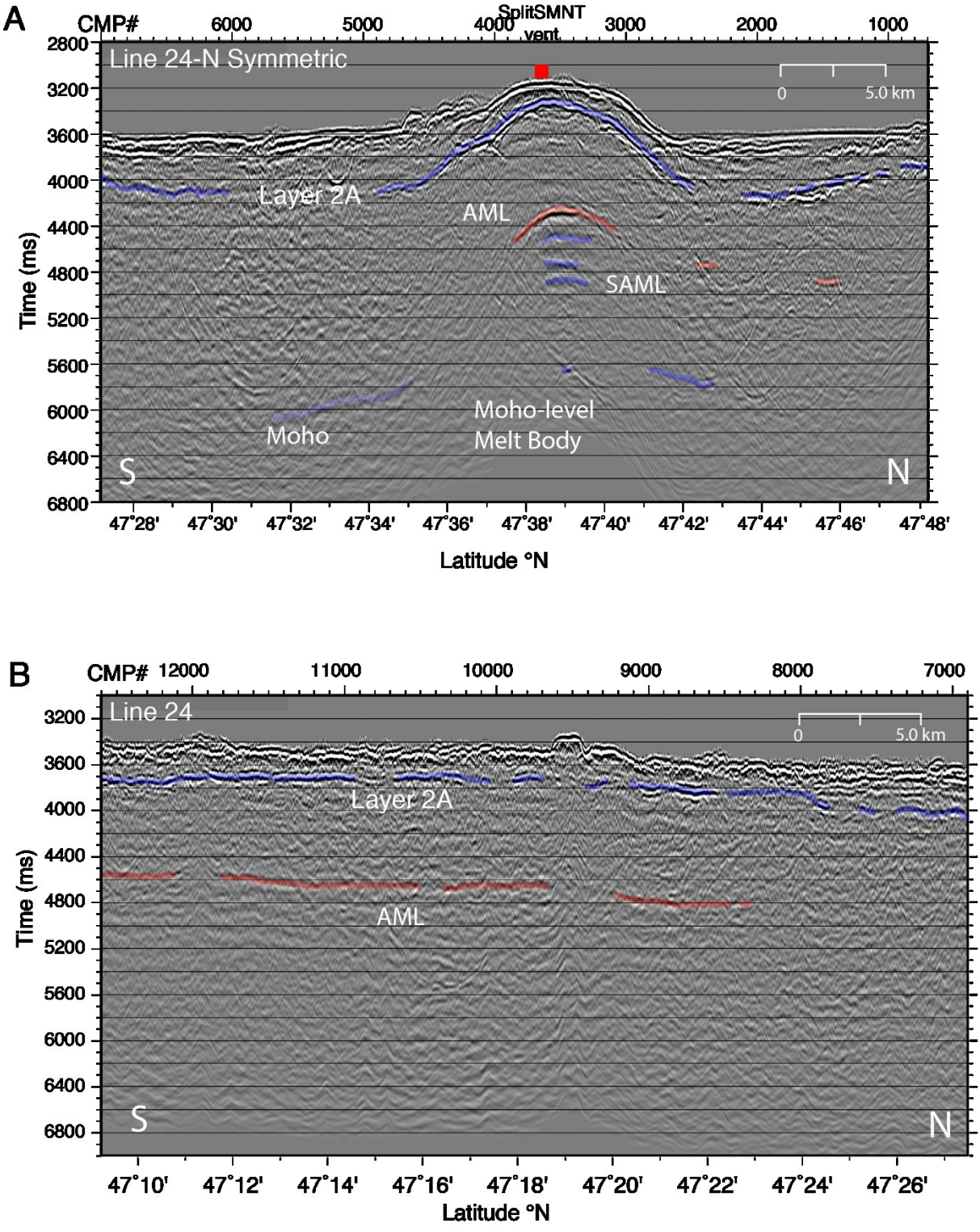

Figure S5. Processed migrated section for line 24 along axis of north portion of Northern Symmetric segment. Locations of hydrothermal vents shown with red squares at top of section. Interpreted horizons are superimposed in semi-transparent line with colors as in

Figure 4. A. Part 1 of section from CDP# 700-7000. B. Part 2 of section from CDP# 6900-12600.

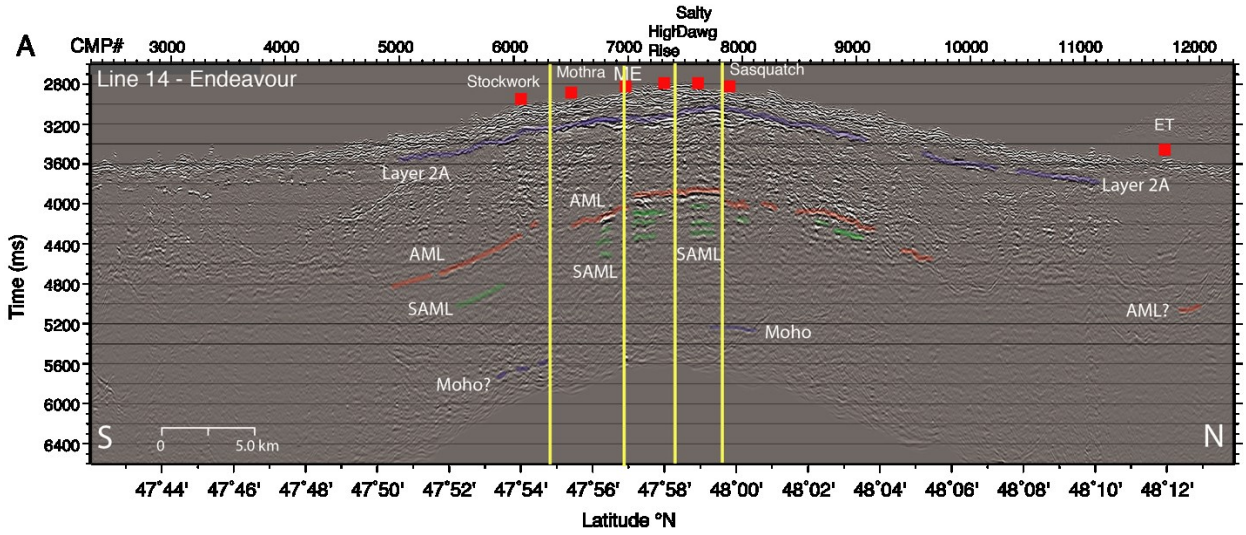

Figure S6. Processed migrated section for line 14 along axis of Endeavour segment. Locations of hydrothermal vents indicated with red squares at top of section. Interpreted horizons are superimposed in semi-transparent line with colors as in Figure 4. Yellow vertical lines indicate boundaries of third-order spreading segments identified along Endeavour segment (discussed in Arnoux et al., 2019).